Modulation of proximity to criticality enhances slow activity fluctuations during free recall

Yellin D[1]., Siegel N.[2], Malach R[1]., Shriki O.[2,3]

[1] Department of Brain Sciences, Weizmann Institute of Science, Rehovot, Israel

[2] Department of Computer Science, Ben-Gurion University of the Negev, Beer-Sheva, Israel

[3] Department of Cognitive and Brain Sciences, Ben-Gurion University of the Negev, Beer-Sheva, Israel

Abstract

Categorically bounded free recall is a fundamental, yet poorly understood capability of human behavior. Thus, we are able to easily engage in spontaneous generative thought processes while constraining them within specific categorical boundaries. For example, easily and freely come up with names of famous politicians while avoiding the intrusions of names of places or movie actors. Previous research has uncovered a neuronal baseline shift mechanism by which ultra-slow spontaneous fluctuations in activity of neurons, participating in the targeted category, get amplified; thus, increasing their probability of crossing the decision bound and initiating the spontaneous event. However, it is not clear how, mechanistically, such amplification may take place in the brain. More generally, it is still unknown how the observed ultra-slow time scales of the scale-free spontaneous fluctuations spectrum emerge out of the typically fast time scales of cortical neurons. Here we show, using a model of a simple random recurrent neuronal network, with its parameters preset near the dynamical phase transition point, that such selective amplification of slow frequencies can be simulated by a small shift of the network closer to its critical point. Hence, an observed byproduct of a shift towards the dynamical phase transition point is the, so called, “critical slowing down” phenomenon. Furthermore, using simple and physiological parameter fitting, with an input consisting of stochastic white noise to the network’s neurons, we precisely simulate the ultra-slow spontaneous fluctuations observed during rest and an intrinsic recall process in the human cortex. Our results illustrate how the complex spontaneous fluctuations observed in the human brain can be explained by a simple, stochastically driven, recurrent network which operates near a critical point. They also provide a ready neuronal mechanism accounting for the remarkable ability of the human brain to set categorical boundaries rapidly and flexibly through amplification of the slow frequencies of the spontaneous, resting state, fluctuations during targeted free behaviors.

Introduction

Human free behavior (i.e., self-generated, spontaneous action), is a fundamental attribute of human nature, underlying many aspects of human creativity and original insights. However, compared to controlled, stimulus–response behaviors, its neuronal underpinnings are far less studied and not as well understood. We have proposed in previous works (Moutard et al., 2015; Norman et al., 2017) that the well-studied and ubiquitous ultra-slow spontaneous activity fluctuations – also termed "resting state" activity (Raichle, 2011) – constitute a universal cortical mechanism that (among other functions) drives free and creative behaviors in the human brain. In the rest of the manuscript, we will refer to these ubiquitous cortical phenomena as spontaneous fluctuations. The power spectrum of these spontaneous activity fluctuations has been precisely characterized, using intra-cranial recordings, as obeying a power-law profile (He, 2014; Miller et al., 2009; Nir et al., 2008). They emerge in well-defined networks across the entire cortex (Buzsáki, 2006; Fox & Raichle, 2007; Nir et al., 2006) and uncover unique patterns of functional connectivity which we and others have proposed reflect habitual task activations and personality traits (Eldar et al., 2013; Gilaie-Dotan et al., 2013; Hahamy et al., 2015; Harmelech & Malach, 2013; Smith et al., 2015; Wilf et al., 2015). They have also been linked to other spontaneous behavioral manifestations such as spontaneous fluctuations in pupil diameter (Yellin et al., 2015) and spontaneous eye-drifts (Ramot et al., 2011). Recently, we have demonstrated a direct link between the spontaneous activity fluctuations and free and creative verbal behaviors (Broday-Dvir & Malach, 2021).

However, a crucial aspect of free behavior is the rapid and flexible control we seamlessly apply when delineating the boundary within which our free behaviors operate. Thus, among countless other examples, jazz musicians can restrict their improvisation specifically to the music domain and to specific scales or jazz styles, whereas an improvising dancer will exert the spontaneous behavior within the domain of motor movement and within specific dancing styles.

If a modulation of the slow spontaneous fluctuations indeed underlies free behaviors - a mechanism should be readily available in the brain to execute such boundary setting regulation on these fluctuations. Indeed, in a study directly aimed at exploring such mechanisms in the domain of free visual imagery and recall, Norman et al. (2017) have

demonstrated that the resting state fluctuations display an increase in the baseline and power of the slow spontaneous fluctuations, which appears specifically in the neuronal groups representing the categories targeted by the free recall task but not in the non-targeted category (see Norman et al., 2017). Such local baseline spectral shift of the spontaneous fluctuations was predicted to bring the targeted neurons closer to the decision threshold, and in this manner greatly enhance the probability of the free behaviors to be expressed strictly within the boundaries of the category intentionally targeted by the individual.

However, whereas these complex neuronal phenomena have been well characterized at high spatial and temporal precision, we are still in the dark as to the neuronal mechanisms that underlie them. Specifically, it is not clear how the characteristic power spectrum of the spontaneous fluctuations - dominated by ultra-slow frequencies - emerges out of the typically fast neuronal elements. Furthermore, it is not clear what is the neuronal mechanism that drives the baseline shift and the selective slow-frequency amplifications that are observed in targeted free behaviors.

Near-critical dynamics as a potential mechanism. Here, we rely on the hypothesis that the cortex operates near criticality (Beggs, 2022; Beggs & Plenz, 2003; Kinouchi & Copelli, 2006; Shew et al., 2009) and propose that these phenomena can be explained in the context of a fundamental property of near-critical recurrent systems - the slowing down and increased slow-frequency amplitude of stochastic fluctuations as these systems approach criticality. Termed “critical slowing down” (Lee et al., 2014; Meisel et al., 2015; Scheffer et al., 2009), the phenomenon describes the universal tendency of systems near a transition point in their dynamics to exhibit slower time scales and take longer time to relax to a steady state equilibrium following perturbations.

Several experimental and theoretical lines of evidence from recent years support the idea that the healthy cortex operates near a critical point in its dynamics, namely close to a boundary between different dynamical phases, exhibiting slow time scales and scale-free dynamics (Arviv et al., 2015; Deco & Jirsa, 2012; Haimovici et al., 2013; Linkenkaer-Hansen et al., 2001; Shew & Plenz, 2013; Shriki et al., 2013; Yu et al., 2013). Scale-free spatiotemporal cascades of neuronal activity, termed neuronal avalanches, have been found in *in vitro* and *in vivo* animal studies as well as in large-scale human fMRI, EEG and MEG recordings (Arviv

et al., 2015; Lombardi et al., 2021; Palva et al., 2013; Tagliazucchi et al., 2012). These avalanches can be well described by the framework of critical branching processes (Harris, 2012). Other studies indicated edge-of-chaos criticality (Bertschinger & Natschläger, 2004; Legenstein & Maass, 2007; Toker et al., 2022). Importantly, near-critical dynamics optimizes information processing (Shew et al., 2009; Shriki & Yellin, 2016) and deviations from critical dynamics are associated with disorders in information processing (Arviv et al., 2016; Dotan & Shriki, 2021; Fekete et al., 2018, 2021). We have previously demonstrated the phenomenon of critical slowing down (CSD) in a recurrent network model of early visual processing (Shriki & Yellin, 2016). As the recurrent network evolves during its learning process, it approaches a critical point in its dynamics and the effective time scales grow longer. For a recent review of critical brain dynamics, see (Beggs, 2022; O'Byrne & Jerbi, 2022).

Network model and tuning of proximity to criticality. To explore this suggested mechanism, we have simulated a simple random recurrent network of rate-based units configured at varying proximity to its critical point. In previous work (Shriki et al., 2003), we have shown that such rate-based models can be rigorously derived from large-scale conductance-based networks that model cortical dynamics. Our network architecture is adapted from the one proposed by (Chaudhuri et al., 2018) to simulate intra-cranial EEG (iEEG) dynamics. Importantly, the proximity of the network model to the critical point can be precisely controlled by tuning relevant parameters. As suggested by (Chaudhuri et al., 2018), proximity to criticality is required to reproduce the observed scale-free power spectrum of iEEG recordings. We speculate that the unique dynamics, as observed by (Norman et al., 2017) during free recall, may be accounted for by setting the model further closer to its critical point.

To provide further insight and intuition into the phenomenon of critical slowing down, both in the context of a recurrent neural network and more generally, Figure 1 provides a schematic illustration of this topic. Panel 1A delineates the expected activity in a random recurrent network at varying proximity to its critical point, namely to the point where the network gain (also termed 'control') parameter is set to $G = 1$. For a transient stimulus, activity in the network (left response panels) will (a) dissipate when the network gain parameter is set to $G < 1$ (see blue arrow), (b) diverge to the maximal neuronal rate (in black dashed line) when $G > 1$ (see green arrow), and (c) tend to persist at enhanced slow

fluctuation frequencies when G $\lesssim$ 1, namely slightly below the critical point (see yellow arrow). For a continuous signal, the steady-state power spectrum indicates an increase in the amplitude of slow-wave activity only at the domain of G $\lesssim$ 1 (right response panel). Figures 1B & 1C provide further illustration of the CSD phenomenon using a one-dimensional non-linear system near its critical (bifurcation) point. In the illustrated system, as depicted in Fig. 1B, the dynamics are characterized by a simple quadratic equation: $\mathrm{f}(x) = x^2 + r$, where x is a time-dependent variable satisfying $\frac{dx}{dt} = \mathrm{f}(x)$, and r is the system's control parameter. In a given simulation, the value of r is kept constant, but its value is used to tune the system towards (or away from) the system's critical point. It can be shown that in this system, a qualitative change in the dynamics of the system occurs at $r = 0$, or in other words - a bifurcation takes place at this critical point. In this sense, the system can be considered as: (a) super-critical, for $r > 0$, since at this domain there are no fixed points and x always diverges to infinity, and (b) sub-critical when $r < 0$ for which two fixed points arise at $x^* = \pm\sqrt{r}$, i.e. when set to those points, x remains fixed over time. The stability can be determined by the derivative of the function f at the fixed point. A stable fixed point is associated with negative derivatives of f and an unstable fixed point is associated with positive derivatives of f, as x approachesx^*. The negative fixed point is stable (following a small perturbation, the dynamics drive x back to the fixed point) whereas the positive fixed point is unstable (small perturbations are amplified). Close to a given fixed point, the dynamics can be linearized and the deviation from the fixed point can be approximated by $\mathrm{e}^{\mathrm{t}/\tau}$, where $\tau = 1/\mathrm{f}'(x^*)$. As the value of the control parameter r approaches 0 from below, the two fixed points coalesce into a single fixed point, which then disappears for $r > 0$ (Figure 1B). The key point is that the magnitude of the time constant that controls the dynamics approaches infinity as r approaches the critical value of 0 (Figure 1C). Thus, the dynamics slow down as the system approaches its critical point.

Summarizing shortly, we suggest that the unique dynamics, as observed by (Norman et al., 2017) may readily be accounted for by a closer proximity of the relevant local cortical network to a critical point during free recall. This enhances the gain of the local network, making it more sensitive to the influence of external noise and driving it to generate patterns that reflect stored memories.

To that end, we propose a model of a randomly connected non-hierarchical recurrent network, subject to an ongoing “intrinsic” membrane potential noise. The activity of this model resembles spontaneous cortical activity and can be compared to the empirical data. For details of the firing rate model equations underlying unit dynamics with the context of the entire network configuration, see Methods.

Our findings, as shown in later sections of this paper, fit the empirical data and indeed support the hypothesized near-criticality slowing down modulation of the signal. Thus, we propose that the phenomenon of scale-free resting state fluctuations and its modulation during intrinsically motivated tasks do not necessitate complex and elaborate cortical organizations and computations, but rather reflect a very basic and ubiquitous behavior common to all suitably configured recurrent systems.

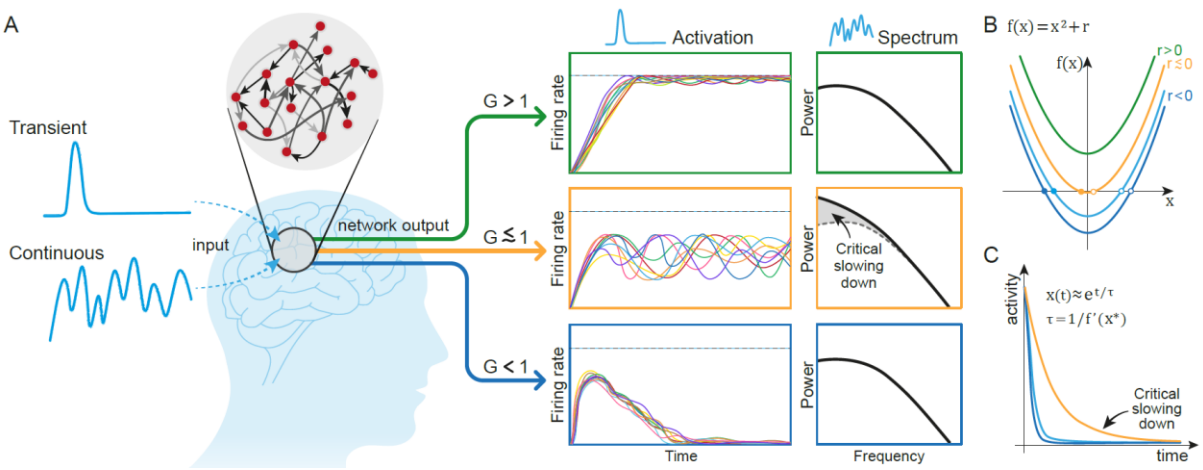

Figure 1. The impact of gain change on the dynamics of a recurrent system. The figure provides an illustrative and simplifying explanation of the critical slowing down (CSD) phenomenon in the dynamics of a recurrent system. CSD takes place as the system crosses between its sub-critical domain (G < 1, here depicted in blue) and its super-critical domain (G > 1, here in green). In this near-critical state (G ≲ 1, here depicted in yellow), when the system’s gain (also termed ‘control’) parameter is increased to the vicinity of (but still below) the critical point, it displays cardinal slowing down and amplification of its dynamics. Panel 1A delineates the expected activity in a random recurrent network at varying proximity to its critical point. For a transient stimulus, activity in the network will (a) dissipate in the sub-critical domain (G < 1, in the bottom sub-panel) (b) diverge to the maximal neuronal rate (black dashed line) in the super-critical domain (G > 1, top sub-panel) and (c) tend to become persistent as the gain approaches G ≲ 1 (middle sub-panel). For a continuous signal, the power spectrum will indicate rise in the amplitude of slow-wave activity only at the domain of

G $\lesssim$ 1. Figures 1B & 1C provide further illustration of the CSD phenomenon exploring the dynamics of a simple one-dimensional non-linear system, driven by the quadratic equation of $f(x) = x^2 + r$. Panel 1B depicts the system and its solutions as the value of r, the control parameter is modified between super-critical (r > 0, in green), sub-critical (r < 0, blue) and near-critical (yellow, r $\lesssim$ 0) states. Panel C shows how the system dynamics slows down as r approaches 0. The curve corresponding to r > 0 diverges exponentially (not shown). See a more detailed discussion in the text.

Methods

Random recurrent network as a rate model

Rate models can be derived from the well-studied Wilson-Cowan equations (Wilson & Cowan, 1972). They were explored within the context of iEEG data in recent literature (Chaudhuri et al., 2018; Gao et al., 2020). In previous work (Shriki et al., 2003), we have shown that such rate models can be faithfully derived from large-scale conductance based networks resembling cortical organization. In this type of rate models, the dynamic variable that characterizes the neuronal activity is the firing rate of the neuron, i.e., the number of electrical pulses (action potentials) in a unit of time. The simplicity of rate models makes them highly useful in studying properties of large networks.

Here, we considered a random recurrent network model consisting of N rate-based units representing single neurons or groups of neurons (see Figures 2-6). We closely follow the model proposed in (Chaudhuri et al., 2018) to explain the power spectrum of iEEG recordings. The firing rate dynamics of the *j*-th neuron's output over time in this model is given by:

$$\tau \frac{d}{dt} r_j(\mathrm{t}) = -r_j(t) + \gamma \left[\sum_{j=1}^{N} W_{jk} r_j + I_j^{ext}(t) \right]_+ \qquad j = 1 \dots N \qquad (1)$$

where r_j is the firing rate of the *j*-th unit activity level, and τ is a characteristic integration time. The $[\ ]_+$ brackets denote a rectified linear (ReLU) activation function. The γ variable denotes the slope of the firing rate – current curve (f-I curve). The weights W_{jk} describe the strength of the connection from the presynaptic unit k to the postsynaptic unit *j*, and I_j^{ext}

denotes the external input to the *j-th* unit (drawn here randomly from a "standard normal" distribution).

Criticality in the random recurrent network

We consider a network architecture comprising a non-hierarchical cluster of recurrently connected neurons characterized by a semi-linear f-I curve with gain γ. Following (Chaudhuri et al., 2018), we choose the connections in this network (the entries of matrix *W*) to be sparse and random. More specifically, each entry is nonzero with probability *p*, and the nonzero entries are drawn from a normal distribution, with positive mean μ_{conn} and variance σ_{conn}, normalized by the size of the network, N.

When set as a rate model (assumed to be represented by the iEEG high-frequency broadband power modulation), we hypothesize it depicts the summed recurrent synaptic current into a fraction of neurons in this network, along with an intrinsic complementary membrane noise. Previous work (Chaudhuri et al., 2018) demonstrated how the product of three main parameters control the proximity to the network's critical branching point. These are: μ_{conn}, γ, and *p.* At the tipping point of criticality, they satisfy the relation $\gamma p \mu_{conn} = 1$, see (Chaudhuri et al., 2018). Thus, we define a control parameter $G = \gamma p \mu_{conn}$, and require that it lies in the vicinity of the critical point - $G \lesssim 1$. In a near-critical state, either one of these arguments composing the control parameter could be varied to yield similar results towards the crossing point into a supercritical state.

To provide additional insight in the present context, we note that near a steady-state, an algebraic linearized approximation of the spontaneous fluctuations dynamics can be obtained. We briefly summarize the details given in (Chaudhuri et al., 2018):

1. The eigenvalue spectrum of such random matrices is composed of a cluster of complex eigenvalues with negative real part, and a single isolated eigenvalue, which corresponds to the uniform eigenvector (namely, to the mean network activity).
2. This approximation is characterized by a matrix whose dominant eigenvalue converges ever closer to 0 as the system approaches its bifurcation point.

Critical slowing down is manifested in the system's temporal dynamics, as they are linked to the inverse of the abovementioned dominant eigenvalue (see SI for additional detail). As the

system approaches criticality, signals reverberate in the network for increasingly longer time, producing a slowly decaying autocorrelation function and increasing the power of low frequencies.

For sake of convenience, the following parameters were kept fixed across all simulation runs presented in the paper: μ_{conn} = 49.881 pA/Hz, σ_{conn} = 4.988 pA/Hz, p = 0.2. Unless otherwise noted, the parameter that was used to control the proximity to criticality was the slope of the f-I curve, γ. We did however verify that qualitatively equivalent results can be reached by modifying G using other parameters.

The characteristic integration time and PSD profile's pattern

As for the characteristic integration time τ, we explored values in the range of 2 – 200 ms. Using a simple linearized mathematical approximation (see SI Figure S1 and (Chaudhuri et al., 2018)) it can be shown that the commonly observed "knee"-bend in in the power spectral density (PSD) profile appears near $f_{knee} = \frac{1}{2\pi\tau}$, and that modulation of slow-frequencies is also significantly influenced by this the integration time constant, implying that the fit tuning process should carefully consider its setting.

Our findings here indicate that using the previously reported timescale of the membrane time constant in the proximity of τ = 20 ms (Gao et al., 2020; Koch et al., 1996; Softky & Koch, 1993) led to an optimal fit regarding the location of this knee in the activity rate PSD curve as well as the related slow frequencies slope. That is, for both of the cases explored in (Nir et al., 2008; Norman et al., 2017), as demonstrated in Figures 2 and 3 respectively.

The parameter α, defined as the fraction (i.e. 0 < α < 1) of network nodes selected for summation, plays a significant role in determining the slope of medium range frequencies (> 0.1 Hz and < 10 Hz) in the PSD curve, since it influences the mixture of slow and fast dynamical modes exposed in the system. When constructing the PSD, we sum the activities of α*N* random nodes and compute the spectrum of the summed activity. The larger the value of α, the larger the contribution of the dominant slow mode to the mid-range PSD slope, since this mode is shared among the network nodes.

Simulation and parameter fitting efforts

Simulation code, including full implementation of the rate model and plotting of figures, was developed in Python, taking advantage of suitable open-sourced libraries' methods (including, but not limited to, SciPy and Matplotlib), facilitating tuning efforts for fitting the empirical results (details below).

For the results depicted in Figure 2, the signal was low-pass filtered (for < 0.1 Hz) as in (Nir et al., 2008), using a Butterworth method. Correlation, auto- and cross-correlation coefficients were computed using time-lagged correlation methods. In panel 2b, the activity of two arbitrarily selected highly-correlated neurons is presented. In panel 2d, the power spectrum was computed using Matplotlib mlab's PSD, implementing the Welch method. A simple amplitude scaling factor k was applied to match the Welch method results with those presented by direct use of FFT power in (Nir et al., 2008). A regression line curve was fitted using a curve-fitting method in the range of 0.1 – 10 Hz.

For Figure 3, the simulation was arranged as consecutive "rest" vs "free-recall" 1800 s blocks. Additive noise I^{add} was defined as constant value within each simulation run, so that $I_{new}^{etx} = I^{ext} + I^{add}$. For the purpose of sampling a satisfactory distribution for statistical analysis, the simulation was repeated using different random seed values. The multiple realizations generated were independently compared with the empirical data. The statistical analysis results for this comparison are demonstrated in SI Figure S3. Other than that, similar simulation and computational methods were applied as in Figure 2. Testing for various possible confounds, the simulation configuration for the results presented in Figures 4 – 6 was suitably adapted, but remained similar in concept to the settings in Figure 3. In data preparation for Figure 5, white noise was sampled in advance, applying suitable filters (using scipy signal.butter methods) over the random (white noise) normal distribution based temporal signal. For the map presented in Figure 6, we iterated through the parameter space of network connectivity and size, iteratively generating random network realizations of larger and larger scale. Thus, as the control parameter G was modified (via γ) from subcritical to near-critical range, values of the slow (normalized by fast) frequency power modulation were collected.

The human iEEG data and its analysis

The empirical data used in this study has been previously reported in (Nir et al., 2008 and Norman et al., 2017). In both studies, intracranial recordings were obtained from patients with pharmacologically resistant epilepsy who were undergoing a surgical evaluation process for the treatment of their condition. In the first study (Nir et al., 2008), data were recorded from five participants (over multiple sessions) under the conditions of wakeful rest. During the wakeful rest, subjects' eyes were closed and the room was dark and quiet, however, alertness was occasionally monitored. The second study (Norman et al., 2017) included twelve participants who performed a free recall task, as follows. Immediately after a 200 s period of closed-eyes resting state, participants were presented with 14 different pictures of famous faces and popular landmarks in a pseudorandom order (each picture was repeated four times, and shown for 1500 ms, with 750 ms inter-stimulus interval). After viewing the pictures, participants put on a blindfold (or closed their eyes) and began a short interference task of counting back from 150 in steps of 5 for 40 s. Upon completion, recall instructions were presented, guiding the patients to recall items from only one category at a time, starting with faces in one run and with places in a second run. Participants were asked to verbally describe each picture they recall, as soon as it comes to mind, with 2–3 prominent visual features. The duration of this free recall phase was 2.5 min per each category. In both experiments analyses of iEEG data were focused on changes in high-frequency broadband amplitude (HFB, also known as high-gamma, defined as the range 40-100 Hz in the first study and 60-160 Hz in the latter one), shown to be a reliable marker of local neuronal population activity (Nir et al., 2007).

Results

To model the iEEG signal, we simulated a sparse random recurrent network, realizing a firing rate model (see Methods). The summed activity of a sample of units represented the corresponding iEEG. The proximity to criticality was modulated through a control parameter, G, corresponding to the product of the network sparseness p, the neural gain, γ, and the mean synaptic strength μ_{conn}, with the critical transition from subcritical to supercritical domain expected at $\gamma p \mu_{\text{conn}} = 1$. We first examined whether the typical dynamical

characteristics of the spontaneous resting state activity fluctuations as recorded in the human cortex could be reproduced by this network model. As can be seen in Figure 2- indeed, the model exhibited similar dynamics when set relatively close to its critical point, namely when the gain parameter was set to G = 0.94.

Figure 2 a-b depict a comparison between real iEEG recordings and simulated network dynamics. Panel 2a shows examples of the spontaneous fluctuations recorded from two isolated homologous auditory sites in the two hemispheres during quiet rest (obtained from Nir et al., 2008). Panel 2b shows, for comparison, examples of similarly correlated activity fluctuations of two simulated units in the recurrent network.

A more comprehensive qualitative comparison across the entire data set is shown in Figure 2 c-d. Here, instead of single neurons we use the broad band high frequency power fluctuations of the intra-cranially recorded local field potential (see Methods). It has been previously shown (Manning et al., 2009; Mukamel et al., 2005; Nir et al., 2007) that these fluctuations in power of the LFP in the high frequency broadband (HFB) provide a reliable index of the fluctuations in the average firing rates of neurons within the recording site. Note that this measure of high frequency power modulations should be distinguished from the direct measure of fluctuations in the LFP signal itself. Panel 2c shows the autocorrelation PSD of the HFB during quiet rest (black line) as well as the cross-correlation PSD function of measurements from auditory cortex obtained across the two hemispheres (orange line). Panel 2d depicts, for comparison, our simulation of these activity fluctuations, obtained in a network of 400 neurons, with the probability for nonzero network connectivity set at $p = 0.2$, and the mean synaptic strength $\mu_{conn} = 49.881$ (note that both parameters were kept fixed in all simulation results presented in this study). We set out to find an initial optimized setting for τ - the decay constant. Having explored various values of τ in the range of 2 – 200 ms (see SI Figure S2), we found the location of the curve's knee frequency was optimized when setting this parameter around 20 ms, which is close to well-known estimates for cortical neurons' membrane time constant (Gao et al., 2020; Koch et al., 1996; Softky & Koch, 1993). The gain parameter controlling the f-I curve slope was set at, γ = 0.094 Hz/pA (implying G = 0.9377 for the control parameter), and the fraction of the network sampled (determining slope of the faster modes) was set at α = 0.05 (see additional explanation in Methods). For the power spectra of the auto- and cross-correlation computations, two

distinct random samplings of αN neurons were obtained. Following Nir et al., 2008, the autocorrelation was computed using signals from the first sampling only (resembling a single cluster of neurons in the network), and cross-correlation was computed iteratively between neuron pairs of both samples. Finally, the power spectrum was obtained by computing the mean of these autocorrelation (black line) and cross-correlation (orange line) curves (Methods). As can be seen, while the simulated function was quite similar to the experimental brain recordings, the curve of the simulation slope was somewhat sharper than in the empirical results. Further efforts to improve this fit were left for future work.

Results for the various values of τ explored to optimize the fit of the "knee" bend in the curve are presented in SI Figure S2, showing τ values for 2, 20 and 200 ms. Note the qualitative similarity between the real and simulated data of the knee frequency location for the autocorrelation (black arrow) and cross-correlation (orange arrow) at τ = 20 ms (denoted by arrows indicating the location of the knee in the empirical results), relative to alternative settings.

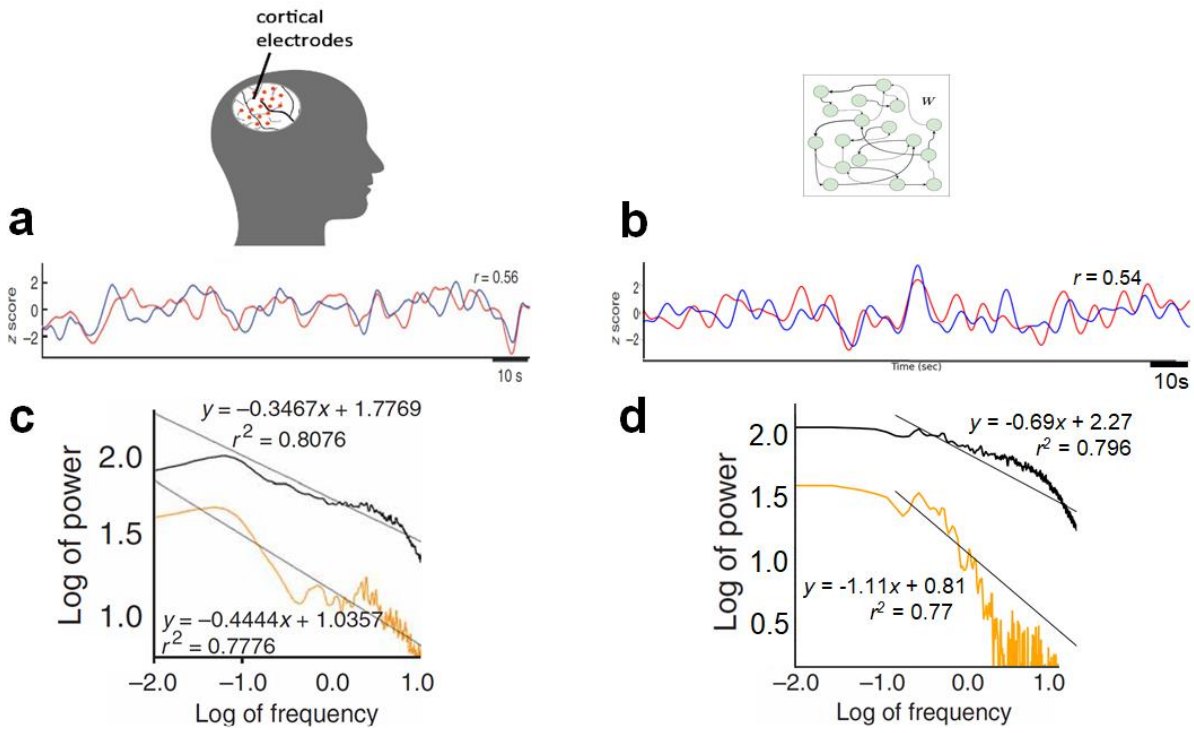

Figure 2. Ultra-slow spontaneous oscillations of neuronal activity in the brain and in a recurrent network simulation. Empirical iEEG results during wakeful-rest (adapted from Nir et al., 2008), presented here in panels a and c, are compared and contrasted with corresponding fitted simulation results in panels b and d, respectively, from an artificial neural

network model with 400 neurons. Panel a presents the HFB signal from homological left and right auditory cortices. Panel b demonstrates a corresponding signal from two highly correlated neurons in the artificial network. Panel c presents the autocorrelation (black line) of the HFB PSD and the cross-correlation (orange line) of this signal obtained across the two auditory cortex hemispheres. Panel d depicts, for comparison, our simulation of these activity fluctuations. Note the similar location of the knee frequency in the spectra of the empirical and simulated data (for further comparison see SI figure S2).

Next we examined whether the recurrent network simulation, using the same value of τ (i.e. 20 ms) could also fit the baseline shift and amplitude amplification of the slow spontaneous fluctuations observed during targeted free behavior, as reported in (Norman et al., 2017). To that end, parameters of the simulated network were again fitted for optimal power spectrum match with results obtained by the intracranial HFB signal PSD.

Figure 3 compares the intra-cranially recorded HFB baseline shift amplification with the simulated neuronal activity. The simulated network consisted of 240 neurons, with parameter settings for p and μ_{conn} remaining fixed with the same values used in the former simulation presented in Figure 2. As for the setting of the decay constant, in addition to the optimal knee-location fit obtained in Figure 2 (with τ = 20 ms), another approximation method was employed, a Lorentzian approach, following (Chaudhuri et al., 2018). The result of this approximation is shown in SI Figure S1. It was established once again, based on both methods, that setting this parameter near the biophysically-grounded-estimate of the membrane time constant optimizes the fit of the knee frequency location, and here also the PSD curve for mid-range frequencies (> 0.1 Hz and < 10 Hz). The sampling fraction was set to α = 0.01 for best adjustment of the curve slope in the faster frequencies. The mean and std of I^{ext}, the noisy membrane potential related input was ~20 (+/- 11.5) pA. The number of steps in the simulation corresponded to 1800 s, of which the first 600 s were omitted as a stabilization period before a stationary signal was achieved (leaving 1200 s for analysis).

Panel 3a depicts an example of the experimentally derived spontaneous HFB fluctuations in two neuronal populations - one that was targeted to elicit free recall (red) and the other that was not targeted (green). The baseline shift of the fluctuations for the targeted area is readily visible. For comparison, Panel 3b shows the simulated activity fluctuations for a network when a uniform baseline (fixed value) shift, I^{add} (see Methods), was added to the white noise inputs (red) and without this added fixed value shift (green). Note the gap

between the two curves can easily be fine-tuned via setting the relative value and ratio of I^{ext} and I^{add}, without compromising other measurable properties.

Panel 3c provides a more comprehensive analysis by showing the PSD, obtained from all intra-cranially recorded sites in the targeted neuronal population (red PSD) vs. the non-targeted population (blue PSD). To make the comparison of these neuronal recordings to the simulations easier, we overlay the simulated results on top of the brain recordings in panel 3d, in which the mean and standard deviation for multiple realizations (specifically, 8 arbitrary random-seed network connectivity initializations) of simulated target (yellow) vs non-target (green) blocks is presented. Here, the fit in PSD was reached by adding a fixed value shift I^{add} of 12.5 pA to the white noise during simulated targeted (orange thick curve) but not to the non-targeted blocks (green thick curve). As in (Norman et al., 2017), the increase in the power of the ultra-slow modulation in the simulated PSD amplitude during recall relative to rest blocks over the different realization was statistically significant (for the range < 0.2 Hz; $p < 0.05$, FDR corrected, signed-rank test).

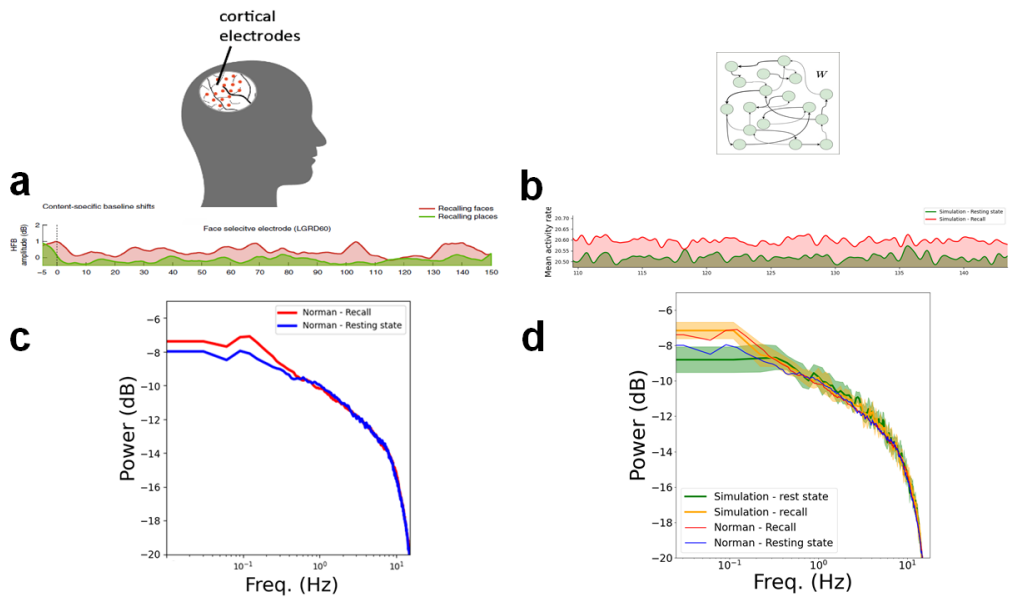

Figure 3. Amplification of slow-fluctuations in the brain and in the recurrent network. iEEG HFB signal from targeted free recall target (red) and non-targeted (green) neuron populations (adapted from Norman et al., 2017) in panel a, is compared with the simulated spontaneous activity in "recall" target (with additive noise) vs non-target "rest" blocks in panel b. The power spectra obtained from all intra-cranially recorded free-recall target sites (red) relative to the non-targeted population (blue) is shown in panel c. Simulated results are overlaid on the empirical PSD results in panel d, showing near fit, in expectation, over

multiple realizations. The mean and standard deviation are shown for the free-recall target (yellow) and non-target (green).

Interestingly, an alternative simulation approach to slowing down the near-critical dynamics led to similar amplification in the targeted ultra-slow frequency PSD. Here a more direct modulation was implemented, increasing the connectional efficacy by a small uniform, fixed, factor. In fact, it was enough to increase the network gain by ~1%, from 0.94 to 0.95, to reproduce the empirically observed enhancement of slow frequencies during free recall. In SI Figure S3 we show distinct single realization PSD results from these simulations using the same color scheme mentioned above. Note the similarity in modulations of the PSD, and, specifically, the amplification in the ultra-slow-frequency domain of the PSD, evident in the targeted relative to non-targeted simulated blocks.

To examine the impact of network connectivity on the PSD in detail we have systematically examined the influence of changing connectivity parameters. This is depicted in Figure 4. In panels 4a-b, a simplified network setting with 100 neurons was used to explore the influence of the connectivity control parameter G, via gradual adjustments of γ, on the spectra while keeping all other network parameters fixed. The simulation lasted 800 s, with the first 200 s omitted in analysis to allow signal stabilization; τ was set to 20 ms, and α was set to 1.0.

Panel 4a demonstrates the impact of setting G across its full end-to-end scope between 0.0 to 1.0, whereas panel 4b focuses on the narrow range as G approaches the critical point of its dynamics. Two important aspects were revealed in this analysis. First, a gradual increase in the amplitude of the slow frequencies that strikingly accelerates as the connectivity value increases, near the dynamical critical point of the control parameter (i.e. when G $\lesssim$ 1). Second, the linear, medium to high frequency range (> ~1 Hz) of the PSD, following an approximate power law function, remained unchanged even when all network connections were set to zero - effectively isolating the neurons from each other. Panel 4c demonstrates the PSD results for the exact same simulation configuration as shown in Figure 3, but in which the levels of baseline shift to the noisy input, I^{ext}, were gradually increased in consecutive realizations. As can be seen, similar to the case of connectivity strength modulation towards criticality in G, the additive noise leads to similar slowing down in the ultra-slow frequencies (only).

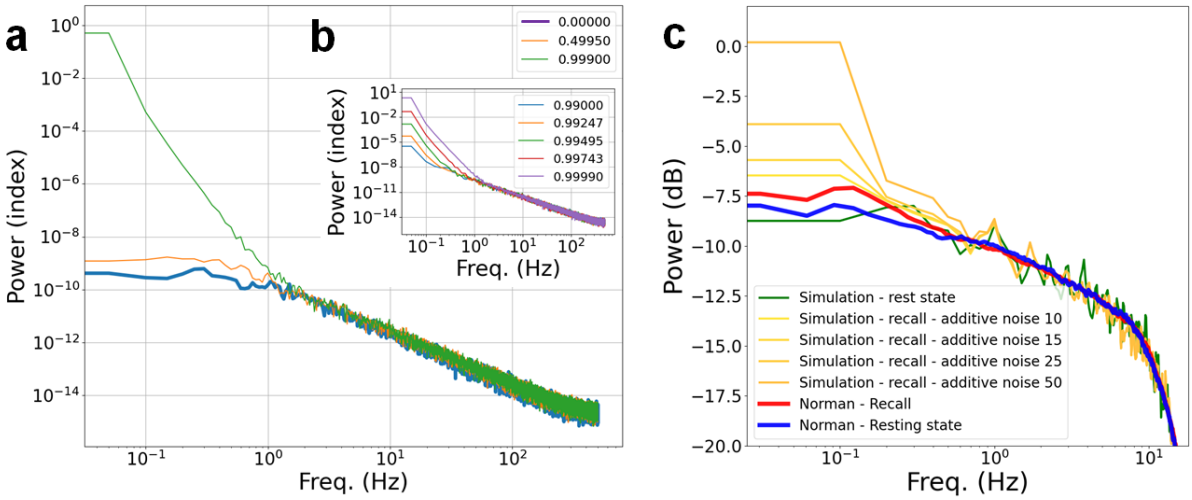

Figure 4. Effect of network connectivity strength and additive noise on spontaneous fluctuations' PSD. Panels a and b demonstrate the critical slowing down of low-range frequencies in an arbitrary network setting as the control parameter approaches the value of 1. In panel a, the case of 0-connectivity (i.e. $\gamma = 0$) is included (blue bold) and in the inset (panel b), the gradual near-criticality slowing down is highlighted. Panel c shows a similar critical slowing down effect, here as a function of the amount of additive noise (see Methods I^{add}) overlaid on PSD results from (Norman et al., 2017).

The emergence of a scale-free power-law in the fluctuations of simulated activity (even in individual isolated neurons) raises the concern that the network behavior merely reflected the dynamical structure of the input noise that was injected to the simulated neurons. To examine this possibility, we modified the profile of the injected noise by high pass filtering and examined how this filtering influenced the network PSD for network parameters near the critical point. The simulation lasted 800 s, with the first 200 s omitted in analysis for purpose of signal stabilization; τ was set to 20 ms, and α was set to 1.0. Figure 5 shows the results of this simulation. The same noise profiles were used also to simulate the activity in a zero-connectivity (isolated neurons) network. The PSD result of this simulation is presented in SI Figure S4.

As can be seen, even drastic changes in the spectral power profile of the input noise had only minor impact on the PSD mid-to high frequency power-law profile of the network as a whole. This is evident in the striking discrepancy between the PSD profile of the input noise (Figure 5 insets c-d) and the PSD of the entire network (panels 5a-b). Of particular interest here is the insensitivity of the network even when all slow input frequencies were drastically quenched to a tenth of its original power (see panel 5a relative to 5c). Similar behavior for

the PSD of mid-to-high range frequencies is preserved also in the isolated neuron network as can be seen in the SI Figure S4 results.

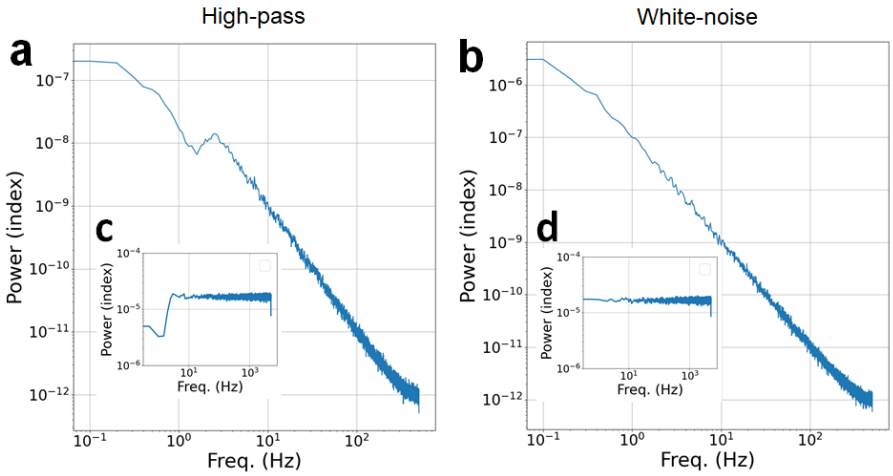

Figure 5. Impact of changes in input noise spectral profile on the network PSD. Panels a-b demonstrate the simulated network PSD when the injected noise is high-pass filtered (panel a) relative to the initial unfiltered white noise (panel b). Insets c – d present the noise spectra in use for each of the main panels, respectively.

To gain a comprehensive insight into the impact of network parameters on the amplification of the spontaneous fluctuations' slow frequencies - i.e. the slowing down near criticality, we scanned the parameter space of network connectivity and size. To this extent, we randomly and iteratively generated network realizations of larger and larger scale, and gradually modified the control parameter G (via γ) from subcritical to near-critical range, while collecting the slow (normalized by fast) frequency power values.

This led to the formation of a two-dimensional heat map as shown in Figure 6. The x and y axes in this map depict network size and control parameter settings, respectively, whereas the color per pixel denotes the degree of slow frequency amplification (more details in Methods). The figure depicts the impact of these two parameters on the increase in slow frequencies.

As can be seen - both parameters had a powerful amplification effect on the slow-frequency power. Amplification became more pronounced only when approaching criticality (i.e. G > 0.95), but interestingly, this was limited to networks larger than 10 neurons. Small networks often showed a mild reduction in slow frequencies near the dynamical transition point.

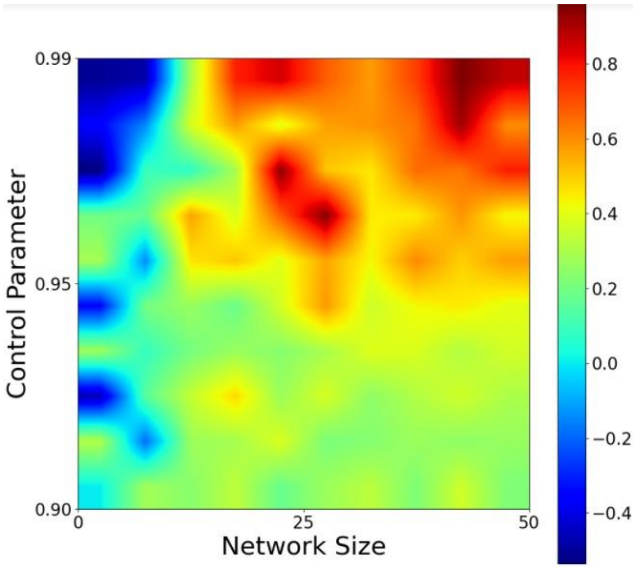

Figure 6. The impact of network size and network connectivity strength on the amplification of the slow spontaneous activity fluctuations. The map color scheme presents this amplification as slow frequency power, normalized by fast frequency power. Each of the cells represents an average of five random realizations, per specific network size and control parameter value.

Discussion

Ultra-slow spontaneous fluctuations of neuronal firing rates (also termed, resting state fluctuations) are one of the most ubiquitous and extensively studied phenomena of the human brain. As outlined in the introduction - numerous studies have revealed that these fluctuations are organized along highly complex but informative connectivity patterns (Fox et al., 2006; Fox & Raichle, 2007; Sadaghiani & Kleinschmidt, 2013; Strappini et al., 2019) suggested to be related to cognitive habits, traits and pathologies (Eldar et al., 2013; Hahamy et al., 2021; Harmelech & Malach, 2013). Recently we have proposed (Broday-Dvir & Malach, 2021; Norman et al., 2017; Norman & Malach, 2022) that these spontaneous fluctuations constitute a universal driver of self-generated, voluntary and creative behaviors.

While there are impressively rich experimental data concerning the properties and dynamical profiles of these slow fluctuations (Fox & Raichle, 2007; Nir et al., 2008; Raichle, 2011; Raut et al., 2021) it is remarkable that the neuronal mechanism that underlies this extremely ubiquitous brain phenomenon is still unknown. It may be argued that since the spontaneous fluctuations are so exceptionally slow and intricately organized - the neuronal

mechanism that underlies them must be equally complex and hence difficult to decipher. Here, we argue that the opposite is the case - at their source the spontaneous fluctuations are driven by an extremely basic physical principle, common to all recurrent systems. Specifically, we propose that it is a general tendency of intrinsic fluctuations in such recurrent networks to slow down in a scale-free manner, and amplify the fluctuations' amplitude as the network approaches its critical phase transition point. This well documented phenomenon is called critical slowing down, and we hypothesize that its fundamental dynamics underlie the observed behaviors of the ultraslow spontaneous fluctuations.

Using a simple random recurrent network along with unstructured noise inputs, we succeeded in simulating critical slowing down dynamics. Importantly, we were able to quantitatively reproduce the intra-cranially recorded neuronal data from the human auditory and visual cortex.

More specifically, by applying a firing rate model of a randomly connected recurrent network of simple neuron units, using biophysically plausible parameter settings, and stochastic inputs, we were able to reproduce the power spectrum of the spontaneous activity fluctuations as reflected in the intracranially measured HFB. We demonstrate that a uniform stochastic white noise input (resembling the stochastic nature of ion fluxes into the membrane potential), along with a physiologically reliable yet simple parameter setting, was sufficient to allow precise simulation of the power-spectra of the spontaneous fluctuations recorded intracranially from the human cortex. Furthermore, a small DC shift in this noise input, or alternatively, a small uniform increase in synaptic efficacy, near the critical transition point of the network dynamics, were sufficient to precisely simulate the amplitude enhancement documented during targeted free recall in the visual cortex.

Based on the success of these simulations we would like to propose that the original driver of the slow spontaneous (resting state) fluctuations in neuronal activity is stochastic noise originating in each individual neuron - which then accumulates through the recurrent connectivity structure. The exact source of this noise is unknown, and may derive from numerous sources - thermal, synaptic, and channel fluctuations (Rusakov et al., 2020; Yarom & Hounsgaard, 2011) – all these processes could drive the random membrane potential

fluctuations consistently found across all types of cortical neurons (Lampl et al., 1999; Raichle, 2011; Yarom & Hounsgaard, 2011).

In the present work, we focused on simulating two major aspects of these spontaneous fluctuations - i.e. their power spectra and its modulation by an intrinsically-motivated task. We have not addressed in these simulations how the complex functional connectivity patterns may emerge out of such noise fluctuations. In the past, we have proposed (Harmelech et al., 2013; Harmelech & Malach, 2013) that these connectivity patterns are shaped by the synaptic structures of the cortical networks and reflect their prior learning. At this stage, we can view this hypothesis as underlying a prediction that could be studied in future simulations, namely, that once a recurrent network consisting of an updatable connectivity based on a suitable learning rule, a repeatedly activated specific pattern (simulating habitual task activations) will spontaneously reappear if the individual network neurons, after it learned the pattern, will be injected with white noise close to criticality. Here, we focus on the other two dynamical aspects of these fluctuations - their power spectral density during rest and its modulation during task-induced targeting of specific categorical boundaries.

Simulation of the power-spectrum of the slow, resting state, fluctuations in a stochastic random recurrent network

Previous studies have revealed the emergence of a scale-free 1/f power-law spectrum using a rate model simulation near criticality (Chaudhuri et al., 2018; Gao et al., 2020). Yet, these earlier studies concentrated only on the near-critical range of the network parameter setting. We set to explore the minimally necessary conditions for this scale-free PSD to arise. This included a study of network connectivity weights far below the critical point in addition to the influence of the profile of intrinsic membrane noise on the network's neuronal activity.

Intracranial recordings of both single neurons as well as the high frequency (gamma) broadband (HFB) amplitudes of the LFP, which has been shown previously to index well the average firing rate of cortical neurons (Manning et al., 2009; Nir et al., 2007), provide a detailed profile of the power-spectra of the spontaneous fluctuations in the human cerebral cortex during rest (see figure 2b and 2c). These spectra consist of two exponents of power-law functions - with the slower frequencies following a shallower exponent compared to the

higher frequencies. Remarkably, a similar profile emerges naturally, under the appropriate parameters, in a random recurrent network whose connection strength and input noise are fully stochastic (compare to figure 3c and 3d). Note that these results were obtained using a minimal number of biophysically-oriented parameter settings, consisting of: (a) a physiologically plausible membrane time constant at ~20 ms (see setting of τ), which appears to provide an optimal fit for the observed HFB PSD; (b) mid-range frequencies in the PSD were best fitted by sampling of only a small part of the network nodes (as conveyed in the setting of α), which is compatible with the localized nature of the empirical recording sites, and, (c) the system's slowing down was controlled by the single gain parameter (G). We will first discuss the high frequency slope of the HFB PSD.

Power-law of stochastic fluctuations at the single cell level

Analyzing the behavior of the network under zero connectivity (see figure 4A) revealed that despite the fact that the spectra of the stochastic noise injected into each neuron was flat (white noise) or even biased towards higher frequencies – the resultant fluctuations in membrane potential after passing through the isolated individual cell's dynamics came out as approximating a power-law beyond a certain "knee" frequency (see Methods and SI figure S4). Thus, the neuron, even when decoupled from the rest of the network, passes the slow frequency band and attenuates the higher-frequencies in a scale-free manner. A mathematical analysis presented in SI section 1, indicates that the dynamics of a scale-free power spectrum with exponent of -2 is indeed the expected result for the fast-mode HFB PSD. Importantly, it should be noted that recent studies of activity fluctuations in isolated cortical and hippocampal neurons reveal that even in the absence of network connections, the biophysical properties of individual neurons are capable of generating stochastic fluctuations obeying scale-free power-law profiles as well as long time-scales (Gal et al., 2010; Gal & Marom, 2013a; Sukenik et al., 2021).

Near-critical recurrent networks amplify the ultra-slow frequencies of the spontaneous fluctuations.

Examining the impact of the network connectivity on the spontaneous fluctuations readily reveals the contribution of the recurrent connectivity – which appears to be a frequency specific amplification of the slow frequencies amplitude in the spontaneous fluctuations spectra, as the network approaches its dynamical phase transition point. This is revealed

when examining separately the impact of changing the connectivity strength- i.e. the efficacy of intra-neuronal communication weight on the one hand, and the richness of the connectivity as reflected in network size, on the other (Figure 6). Importantly, as the figure shows, a successful amplification of slow frequencies can be achieved only within a regime in which these two parameter spaces overlap. When either connection strength is operating in an exceedingly small network of few neurons, or when a relatively large network is set to be subcritical, with relatively weak connectivity, the amplitude of slow frequencies remains relatively low. Yet, it should be noted that only random network configurations were explored in this study. A better structured connectome arrangement, whether shaped by innate prearrangement or as learned by prior experiences, may present other near-critical behaviors. Nevertheless it should be noted that a powerful amplification of ultra-slow fluctuations can be obtained even in extremely small, properly configured, networks possessing < 20 neurons - suggesting that ultra-slow fluctuations lasting many seconds do not necessarily depend on large scale cortical networks for their generation, as also suggested by previous work (Gal & Marom, 2013b).

Modulation of proximity to criticality as a mechanism for boundary setting in free behaviors

As discussed in the introduction, a particularly important aspect of the spontaneous fluctuations is that they can be selectively amplified when spontaneous behavior is intentionally confined to a specific category. Thus, when participants attempt to freely visualize different items belonging to a certain category of visual stimuli, their local slow spontaneous fluctuations get amplified prior to the recall event (See figure 2b and 2c and more details in Norman et al., 2017). Such amplification will naturally enhance the probability of these fluctuations to cross the decision bound in the category-selective area. This provides an elegant mechanism for rapid and flexible control over the expression of any spontaneous behavior within an intentionally selected categorical boundary. Thus, when we try to freely come up with images of different apples, we rarely imagine, by mistake, an orange.

In this scheme, crossing the decision bound may be naturally implemented as a transient, powerful, self-amplification of local populations' activity. These dynamics have been termed "local ignition". Signatures of such local ignitions have been observed experimentally using

iEEG recordings when crossing the perceptual awareness threshold (Fisch et al., 2009; Moutard et al., 2015). Furthermore, in the context of network dynamics, it has been shown that in the vicinity of a critical point, increased network sensitivity (susceptibility) allows it to encode and recall information more effectively by enabling it to respond to inputs and adapt to noise in a more balanced way (Kim et al., 2021; Shriki & Yellin, 2016).

Our random recurrent network simulations demonstrate that the phenomenon of critical slowing down provides a ready and straightforward mechanism by which such slow fluctuations could be selectively amplified. The results clearly show how a simple fixed value shift in the noise level (Figure 2d) or, alternatively, a fixed gain modulation in network connectivity (Figure SI S3) can both accurately reproduce the slow frequency amplification, intra-cranially recorded from the visual cortex of participants during category-selective visual recall.

It is important to note that what appears to be the key factor in inducing this amplification effect is not the specific mechanism that controls the overall network's excitation – we obtained similar results when enhancing the noise input to each neuron individually or, alternatively, when increasing the connectivity across neurons while maintaining their excitation constant. In a network that is already near enough to its dynamical phase transition, a notably small enhancement was sufficient to produce the experimentally observed amplification. The essential parameter that controls the amplitude of the fluctuations is simply how close the network is to its critical transition point.

Differentiating fluctuations in neuronal activity rate from local field fluctuations

It is important to emphasize that both the brain data and recurrent network simulations relate specifically to fluctuations in neuronal firing rate or when these were not available – to the broadband high frequencies (gamma) envelope of the LFP that we and others have shown to reflect fluctuations in average firing rates of local neuronal populations (Manning et al., 2009; Nir et al., 2007). These measures of firing rate fluctuations should be distinguished from fluctuations in the local electrical field, i.e. the LFP, itself. Thus it should be emphasized that the power-spectrum of the LFP is not equivalent and should not be confused with the power spectrum of the firing rate or HFB fluctuations. For example, under different experimental paradigms the two types of fluctuations can in fact be antagonistic to each other (Privman et al., 2011). Another important insight on this matter can be observed

from a “criticality” standpoint. In this regard, previous studies (Chaudhuri et al., 2018; Gao et al., 2020) suggested that LFP power spectra is optimally fitted by setting the dynamics control parameter precisely at the tipping point of criticality (i.e. at G = 1). This could potentially imply fundamental instability, having the network easily cross between subcritical to supercritical states. Interestingly, our optimal fit for the HFB power spectra imply that relevant cortical networks operate below this critical transition point (i.e. at G ~ 0.94), where stability is still maintained. Yet, they operate close enough to critical dynamics allowing the system to computationally benefit from near-criticality effects. We have argued previously, based on intra-cranial analysis of visual responses, that the link between the LFP and firing rates is more appropriately captured by measuring the changes in the exponent of the LFP power-law PSD (Podvalny et al., 2015). These issues could in principle be examined also in our present recurrent network simulations but have not been pursued in this work.

In summary

The phenomenon of slow spontaneous (resting state) activity fluctuations is a highly complex, extensively studied cortical phenomenon whose neuronal origin is unknown. Here we propose, using network simulations, that this is an emergent network phenomenon. Specifically, it can be traced to stochastic processes at the single neuron level that get amplified and shaped by the synaptic structure of the massive cortical recurrent connectivity, at a near-critical state of the network. Our simulations precisely reproduce the power-spectra of these fluctuations as measured from the human cortex during rest and free recall. Furthermore, they provide a ready mechanistic explanation for the observation that targeting of specific categories of behavior amplifies the slow band of the spontaneous activity fluctuations. Our simulations suggest that this neuronal mechanism takes advantage of a common property of recurrent systems - critical slowing down - in which slow frequencies are amplified as the system approaches its dynamical phase transition point.

References

Arviv, O., Goldstein, A., & Shriki, O. (2015). Near-Critical Dynamics in Stimulus-Evoked Activity of the Human Brain and Its Relation to Spontaneous Resting-State Activity. *Journal of Neuroscience*, *35*(41), 13927–13942. https://doi.org/10.1523/JNEUROSCI.0477-15.2015

Arviv, O., Medvedovsky, M., Sheintuch, L., Goldstein, A., & Shriki, O. (2016). Deviations from Critical Dynamics in Interictal Epileptiform Activity. *Journal of Neuroscience*, *36*(48), 12276–12292. https://doi.org/10.1523/JNEUROSCI.0809-16.2016

Beggs, J. M. (2022). *The cortex and the critical point: Understanding the power of emergence*. The MIT Press.

Beggs, J. M., & Plenz, D. (2003). Neuronal Avalanches in Neocortical Circuits. *The Journal of Neuroscience*, *23*(35), 11167–11177. https://doi.org/10.1523/JNEUROSCI.23-35-11167.2003

Bertschinger, N., & Natschläger, T. (2004). Real-Time Computation at the Edge of Chaos in Recurrent Neural Networks. *Neural Computation*, *16*(7), 1413–1436. https://doi.org/10.1162/089976604323057443

Broday-Dvir, R., & Malach, R. (2021). Resting-State Fluctuations Underlie Free and Creative Verbal Behaviors in the Human Brain. *Cerebral Cortex*, *31*(1), 213–232. https://doi.org/10.1093/cercor/bhaa221

Buzsáki, G. (2006). *Rhythms of the Brain*. Oxford University Press. https://doi.org/10.1093/acprof:oso/9780195301069.001.0001

Chaudhuri, R., He, B. J., & Wang, X.-J. (2018). Random Recurrent Networks Near Criticality Capture the Broadband Power Distribution of Human ECoG Dynamics. *Cerebral Cortex*, *28*(10), 3610–3622. https://doi.org/10.1093/cercor/bhx233

Deco, G., & Jirsa, V. K. (2012). Ongoing Cortical Activity at Rest: Criticality, Multistability, and Ghost Attractors. *The Journal of Neuroscience*, *32*(10), 3366–3375. https://doi.org/10.1523/JNEUROSCI.2523-11.2012

Dotan, A., & Shriki, O. (2021). Tinnitus-like “hallucinations” elicited by sensory deprivation in an entropy maximization recurrent neural network. *PLOS Computational Biology*, *17*(12), e1008664. https://doi.org/10.1371/journal.pcbi.1008664

Eldar, E., Cohen, J. D., & Niv, Y. (2013). The effects of neural gain on attention and learning. *Nature Neuroscience*, *16*(8), 1146–1153. https://doi.org/10.1038/nn.3428

Fekete, T., Hinrichs, H., Sitt, J. D., Heinze, H.-J., & Shriki, O. (2021). Multiscale criticality measures as general-purpose gauges of proper brain function. *Scientific Reports*, *11*(1), 14441. https://doi.org/10.1038/s41598-021-93880-8

Fekete, T., Omer, D. B., O’Hashi, K., Grinvald, A., van Leeuwen, C., & Shriki, O. (2018). Critical dynamics, anesthesia and information integration: Lessons from multi-scale criticality analysis of voltage imaging data. *NeuroImage*, *183*, 919–933. https://doi.org/10.1016/j.neuroimage.2018.08.026

Fisch, L., Privman, E., Ramot, M., Harel, M., Nir, Y., Kipervasser, S., Andelman, F., Neufeld, M. Y., Kramer, U., Fried, I., & Malach, R. (2009). Neural “Ignition”: Enhanced Activation Linked to Perceptual Awareness in Human Ventral Stream Visual Cortex. *Neuron*, *64*(4), 562–574. https://doi.org/10.1016/j.neuron.2009.11.001

Fox, M. D., Corbetta, M., Snyder, A. Z., Vincent, J. L., & Raichle, M. E. (2006). Spontaneous neuronal activity distinguishes human dorsal and ventral attention systems. *Proceedings of the National Academy of Sciences*, *103*(26), 10046–10051. https://doi.org/10.1073/pnas.0604187103

Fox, M. D., & Raichle, M. E. (2007). Spontaneous fluctuations in brain activity observed with functional magnetic resonance imaging. *Nature Reviews Neuroscience*, *8*(9), 700–711. https://doi.org/10.1038/nrn2201

Gal, A., Eytan, D., Wallach, A., Sandler, M., Schiller, J., & Marom, S. (2010). Dynamics of Excitability over Extended Timescales in Cultured Cortical Neurons. *Journal of Neuroscience*, *30*(48), 16332–16342. https://doi.org/10.1523/JNEUROSCI.4859-10.2010

Gal, A., & Marom, S. (2013a). Entrainment of the Intrinsic Dynamics of Single Isolated Neurons by Natural-Like Input. *Journal of Neuroscience*, *33*(18), 7912–7918. https://doi.org/10.1523/JNEUROSCI.3763-12.2013

Gal, A., & Marom, S. (2013b). Self-organized criticality in single-neuron excitability. *Physical Review E*, *88*(6), 062717. https://doi.org/10.1103/PhysRevE.88.062717

Gao, R., van den Brink, R. L., Pfeffer, T., & Voytek, B. (2020). Neuronal timescales are functionally dynamic and shaped by cortical microarchitecture. *ELife*, *9*, e61277. https://doi.org/10.7554/eLife.61277

Gilaie-Dotan, S., Hahamy-Dubossarsky, A., Nir, Y., Berkovich-Ohana, A., Bentin, S., & Malach, R. (2013). Resting state functional connectivity reflects abnormal task-activated patterns in a developmental object agnosic. *NeuroImage*, *70*, 189–198. https://doi.org/10.1016/j.neuroimage.2012.12.049

Hahamy, A., Behrmann, M., & Malach, R. (2015). The idiosyncratic brain: Distortion of spontaneous connectivity patterns in autism spectrum disorder. *Nature Neuroscience*, *18*(2), 302–309. https://doi.org/10.1038/nn.3919

Hahamy, A., Wilf, M., Rosin, B., Behrmann, M., & Malach, R. (2021). How do the blind 'see'? The role of spontaneous brain activity in self-generated perception. *Brain*, *144*(1), 340–353. https://doi.org/10.1093/brain/awaa384

Haimovici, A., Tagliazucchi, E., Balenzuela, P., & Chialvo, D. R. (2013). Brain Organization into Resting State Networks Emerges at Criticality on a Model of the Human Connectome. *Physical Review Letters*, *110*(17), 178101. https://doi.org/10.1103/PhysRevLett.110.178101

Harmelech, T., & Malach, R. (2013). Neurocognitive biases and the patterns of spontaneous correlations in the human cortex. *Trends in Cognitive Sciences*, *17*(12), 606–615. https://doi.org/10.1016/j.tics.2013.09.014

Harmelech, T., Preminger, S., Wertman, E., & Malach, R. (2013). The Day-After Effect: Long Term, Hebbian-Like Restructuring of Resting-State fMRI Patterns Induced by a Single Epoch of

Cortical Activation. *Journal of Neuroscience*, *33*(22), 9488–9497. https://doi.org/10.1523/JNEUROSCI.5911-12.2013

Harris, T. E. (2012). *The theory of branching processes*. Springer-Verlag.

He, B. J. (2014). Scale-free brain activity: Past, present, and future. *Trends in Cognitive Sciences*, *18*(9), 480–487. https://doi.org/10.1016/j.tics.2014.04.003

Kim, M., Kim, H., Huang, Z., Mashour, G. A., Jordan, D., Ilg, R., & Lee, U. (2021). Criticality Creates a Functional Platform for Network Transitions Between Internal and External Processing Modes in the Human Brain. *Frontiers in Systems Neuroscience*, *15*, 657809. https://doi.org/10.3389/fnsys.2021.657809

Kinouchi, O., & Copelli, M. (2006). Optimal dynamical range of excitable networks at criticality. *Nature Physics*, *2*(5), 348–351. https://doi.org/10.1038/nphys289

Koch, C., Rapp, M., & Segev, I. (1996). A Brief History of Time (Constants). *Cerebral Cortex*, *6*(2), 93–101. https://doi.org/10.1093/cercor/6.2.93

Lampl, I., Reichova, I., & Ferster, D. (1999). Synchronous Membrane Potential Fluctuations in Neurons of the Cat Visual Cortex. *Neuron*, *22*(2), 361–374. https://doi.org/10.1016/S0896-6273(00)81096-X

Lee, K.-E., Lopes, M. A., Mendes, J. F. F., & Goltsev, A. V. (2014). Critical phenomena and noise-induced phase transitions in neuronal networks. *Physical Review E*, *89*(1), 012701. https://doi.org/10.1103/PhysRevE.89.012701

Legenstein, R., & Maass, W. (2007). Edge of chaos and prediction of computational performance for neural circuit models. *Neural Networks*, *20*(3), 323–334. https://doi.org/10.1016/j.neunet.2007.04.017

Linkenkaer-Hansen, K., Nikouline, V. V., Palva, J. M., & Ilmoniemi, R. J. (2001). Long-Range Temporal Correlations and Scaling Behavior in Human Brain Oscillations. *The Journal of Neuroscience*, *21*(4), 1370–1377. https://doi.org/10.1523/JNEUROSCI.21-04-01370.2001

Lombardi, F., Shriki, O., Herrmann, H. J., & de Arcangelis, L. (2021). Long-range temporal correlations in the broadband resting state activity of the human brain revealed by neuronal avalanches. *Neurocomputing*, *461*, 657–666. https://doi.org/10.1016/j.neucom.2020.05.126

Manning, J. R., Jacobs, J., Fried, I., & Kahana, M. J. (2009). Broadband Shifts in Local Field Potential Power Spectra Are Correlated with Single-Neuron Spiking in Humans. *Journal of Neuroscience*, *29*(43), 13613–13620. https://doi.org/10.1523/JNEUROSCI.2041-09.2009

Meisel, C., Klaus, A., Kuehn, C., & Plenz, D. (2015). Critical Slowing Down Governs the Transition to Neuron Spiking. *PLOS Computational Biology*, *11*(2), e1004097. https://doi.org/10.1371/journal.pcbi.1004097

Miller, K. J., Sorensen, L. B., Ojemann, J. G., & den Nijs, M. (2009). Power-Law Scaling in the Brain Surface Electric Potential. *PLoS Computational Biology*, *5*(12), e1000609. https://doi.org/10.1371/journal.pcbi.1000609

Moutard, C., Dehaene, S., & Malach, R. (2015). Spontaneous Fluctuations and Non-linear Ignitions: Two Dynamic Faces of Cortical Recurrent Loops. *Neuron*, *88*(1), 194–206. https://doi.org/10.1016/j.neuron.2015.09.018

Mukamel, R., Gelbard, H., Arieli, A., Hasson, U., Fried, I., & Malach, R. (2005). Coupling Between Neuronal Firing, Field Potentials, and fMRI in Human Auditory Cortex. *Science*, *309*(5736), 951–954. https://doi.org/10.1126/science.1110913

Nir, Y., Fisch, L., Mukamel, R., Gelbard-Sagiv, H., Arieli, A., Fried, I., & Malach, R. (2007). Coupling between Neuronal Firing Rate, Gamma LFP, and BOLD fMRI Is Related to Interneuronal Correlations. *Current Biology*, *17*(15), 1275–1285. https://doi.org/10.1016/j.cub.2007.06.066

Nir, Y., Hasson, U., Levy, I., Yeshurun, Y., & Malach, R. (2006). Widespread functional connectivity and fMRI fluctuations in human visual cortex in the absence of visual stimulation. *NeuroImage*, *30*(4), 1313–1324. https://doi.org/10.1016/j.neuroimage.2005.11.018

Nir, Y., Mukamel, R., Dinstein, I., Privman, E., Harel, M., Fisch, L., Gelbard-Sagiv, H., Kipervasser, S., Andelman, F., Neufeld, M. Y., Kramer, U., Arieli, A., Fried, I., & Malach, R. (2008).

Interhemispheric correlations of slow spontaneous neuronal fluctuations revealed in human sensory cortex. *Nature Neuroscience*, *11*(9), 1100–1108. https://doi.org/10.1038/nn.2177

Norman, Y., & Malach, R. (2022). *What can iEEG inform us about mechanisms of spontaneous behavior?* [Preprint]. PsyArXiv. https://doi.org/10.31234/osf.io/94vd5

Norman, Y., Yeagle, E. M., Harel, M., Mehta, A. D., & Malach, R. (2017). Neuronal baseline shifts underlying boundary setting during free recall. *Nature Communications*, *8*(1), 1301. https://doi.org/10.1038/s41467-017-01184-1

O'Byrne, J., & Jerbi, K. (2022). How critical is brain criticality? *Trends in Neurosciences*, *45*(11), 820–837. https://doi.org/10.1016/j.tins.2022.08.007

Palva, J. M., Zhigalov, A., Hirvonen, J., Korhonen, O., Linkenkaer-Hansen, K., & Palva, S. (2013). Neuronal long-range temporal correlations and avalanche dynamics are correlated with behavioral scaling laws. *Proceedings of the National Academy of Sciences*, *110*(9), 3585–3590. https://doi.org/10.1073/pnas.1216855110

Podvalny, E., Noy, N., Harel, M., Bickel, S., Chechik, G., Schroeder, C. E., Mehta, A. D., Tsodyks, M., & Malach, R. (2015). A unifying principle underlying the extracellular field potential spectral responses in the human cortex. *Journal of Neurophysiology*, *114*(1), 505–519. https://doi.org/10.1152/jn.00943.2014

Privman, E., Fisch, L., Neufeld, M. Y., Kramer, U., Kipervasser, S., Andelman, F., Yeshurun, Y., Fried, I., & Malach, R. (2011). Antagonistic Relationship between Gamma Power and Visual Evoked Potentials Revealed in Human Visual Cortex. *Cerebral Cortex*, *21*(3), 616–624. https://doi.org/10.1093/cercor/bhq128

Raichle, M. E. (2011). The Restless Brain. *Brain Connectivity*, *1*(1), 3–12. https://doi.org/10.1089/brain.2011.0019

Ramot, M., Wilf, M., Goldberg, H., Weiss, T., Deouell, L. Y., & Malach, R. (2011). Coupling between spontaneous (resting state) fMRI fluctuations and human oculo-motor activity. *NeuroImage*, *58*(1), 213–225. https://doi.org/10.1016/j.neuroimage.2011.06.015

Raut, R. V., Snyder, A. Z., Mitra, A., Yellin, D., Fujii, N., Malach, R., & Raichle, M. E. (2021). Global waves synchronize the brain's functional systems with fluctuating arousal. *Science Advances*, *7*(30), eabf2709. https://doi.org/10.1126/sciadv.abf2709

Rusakov, D. A., Savtchenko, L. P., & Latham, P. E. (2020). Noisy Synaptic Conductance: Bug or a Feature? *Trends in Neurosciences*, *43*(6), 363–372. https://doi.org/10.1016/j.tins.2020.03.009

Sadaghiani, S., & Kleinschmidt, A. (2013). Functional interactions between intrinsic brain activity and behavior. *NeuroImage*, *80*, 379–386. https://doi.org/10.1016/j.neuroimage.2013.04.100

Scheffer, M., Bascompte, J., Brock, W. A., Brovkin, V., Carpenter, S. R., Dakos, V., Held, H., van Nes, E. H., Rietkerk, M., & Sugihara, G. (2009). Early-warning signals for critical transitions. *Nature*, *461*(7260), 53–59. https://doi.org/10.1038/nature08227

Shew, W. L., & Plenz, D. (2013). The Functional Benefits of Criticality in the Cortex. *The Neuroscientist*, *19*(1), 88–100. https://doi.org/10.1177/1073858412445487

Shew, W. L., Yang, H., Petermann, T., Roy, R., & Plenz, D. (2009). Neuronal Avalanches Imply Maximum Dynamic Range in Cortical Networks at Criticality. *Journal of Neuroscience*, *29*(49), 15595–15600. https://doi.org/10.1523/JNEUROSCI.3864-09.2009

Shriki, O., Alstott, J., Carver, F., Holroyd, T., Henson, R. N. A., Smith, M. L., Coppola, R., Bullmore, E., & Plenz, D. (2013). Neuronal Avalanches in the Resting MEG of the Human Brain. *Journal of Neuroscience*, *33*(16), 7079–7090. https://doi.org/10.1523/JNEUROSCI.4286-12.2013

Shriki, O., Hansel, D., & Sompolinsky, H. (2003). Rate Models for Conductance-Based Cortical Neuronal Networks. *Neural Computation*, *15*(8), 1809–1841. https://doi.org/10.1162/08997660360675053

Shriki, O., & Yellin, D. (2016). Optimal Information Representation and Criticality in an Adaptive Sensory Recurrent Neuronal Network. *PLOS Computational Biology*, *12*(2), e1004698. https://doi.org/10.1371/journal.pcbi.1004698

Smith, S. M., Nichols, T. E., Vidaurre, D., Winkler, A. M., Behrens, T. E. J., Glasser, M. F., Ugurbil, K., Barch, D. M., Van Essen, D. C., & Miller, K. L. (2015). A positive-negative mode of population covariation links brain connectivity, demographics and behavior. *Nature Neuroscience*, *18*(11), 1565–1567. https://doi.org/10.1038/nn.4125

Softky, W., & Koch, C. (1993). The highly irregular firing of cortical cells is inconsistent with temporal integration of random EPSPs. *The Journal of Neuroscience*, *13*(1), 334–350. https://doi.org/10.1523/JNEUROSCI.13-01-00334.1993

Strappini, F., Wilf, M., Karp, O., Goldberg, H., Harel, M., Furman-Haran, E., Golan, T., & Malach, R. (2019). Resting-State Activity in High-Order Visual Areas as a Window into Natural Human Brain Activations. *Cerebral Cortex*, *29*(9), 3618–3635. https://doi.org/10.1093/cercor/bhy242

Sukenik, N., Vinogradov, O., Weinreb, E., Segal, M., Levina, A., & Moses, E. (2021). Neuronal circuits overcome imbalance in excitation and inhibition by adjusting connection numbers. *Proceedings of the National Academy of Sciences*, *118*(12), e2018459118. https://doi.org/10.1073/pnas.2018459118

Tagliazucchi, E., Balenzuela, P., Fraiman, D., & Chialvo, D. R. (2012). Criticality in Large-Scale Brain fMRI Dynamics Unveiled by a Novel Point Process Analysis. *Frontiers in Physiology*, *3*. https://doi.org/10.3389/fphys.2012.00015

Toker, D., Pappas, I., Lendner, J. D., Frohlich, J., Mateos, D. M., Muthukumaraswamy, S., Carhart-Harris, R., Paff, M., Vespa, P. M., Monti, M. M., Sommer, F. T., Knight, R. T., & D'Esposito, M. (2022). Consciousness is supported by near-critical slow cortical electrodynamics. *Proceedings of the National Academy of Sciences*, *119*(7), e2024455119. https://doi.org/10.1073/pnas.2024455119

Wilf, M., Strappini, F., Golan, T., Hahamy, A., Harel, M., & Malach, R. (2015). Spontaneously Emerging Patterns in Human Visual Cortex Reflect Responses to Naturalistic Sensory Stimuli. *Cerebral Cortex*, bhv275. https://doi.org/10.1093/cercor/bhv275

Wilson, H. R., & Cowan, J. D. (1972). Excitatory and Inhibitory Interactions in Localized Populations of Model Neurons. *Biophysical Journal*, *12*(1), 1–24. https://doi.org/10.1016/S0006-3495(72)86068-5

Yarom, Y., & Hounsgaard, J. (2011). Voltage Fluctuations in Neurons: Signal or Noise? *Physiological Reviews*, *91*(3), 917–929. https://doi.org/10.1152/physrev.00019.2010

Yellin, D., Berkovich-Ohana, A., & Malach, R. (2015). Coupling between pupil fluctuations and resting-state fMRI uncovers a slow build-up of antagonistic responses in the human cortex. *NeuroImage*, *106*, 414–427. https://doi.org/10.1016/j.neuroimage.2014.11.034

Yu, S., Yang, H., Shriki, O., & Plenz, D. (2013). Universal organization of resting brain activity at the thermodynamic critical point. *Frontiers in Systems Neuroscience*, *7*. https://doi.org/10.3389/fnsys.2013.00042